

E11-2009-178

M. Majerle<sup>1,2</sup>, J. Adam<sup>1,3</sup>, A. Krása<sup>1,2</sup>, S. Peetermans<sup>4</sup>,  
O. Sláma<sup>1</sup>, V. I. Stegailov<sup>3</sup>, O. Svoboda<sup>1,2</sup>,  
V. M. Tsoupko-Sitnikov<sup>3</sup>, V. Wagner<sup>1,2</sup>

MONTE CARLO METHOD IN NEUTRON ACTIVATION  
ANALYSIS

Submitted to «Kerntechnik»

---

<sup>1</sup> Nuclear Physics Institute of ASCR PRI, Řež, the Czech Republic

<sup>2</sup> Faculty of Nuclear Sciences and Physical Engineering of CTU, Prague,  
the Czech Republic

<sup>3</sup> Joint Institute for Nuclear Research, Dubna, Russia

<sup>4</sup> Faculty of Engineering of Ghent University, Ghent, Belgium

Майерле М. и др.  
Метод Монте-Карло в нейтронно-активационном анализе

E11-2009-178

Нейтронно-активационные детекторы являются полезной техникой для измерения нейтронных потоков в экспериментах со спалогенными реакциями. Изучение полезности и точности этой техники в подобных экспериментах выполнено методом Монте-Карло с помощью программ MCNPX и FLUKA.

Работа выполнена в Лаборатории ядерных проблем им. В. П. Дзелепова ОИЯИ.

Препринт Объединенного института ядерных исследований. Дубна, 2009

Majerle M. et al.  
Monte Carlo Method in Neutron Activation Analysis

P11-2009-178

Neutron activation detectors are a useful technique for the neutron flux measurements in spallation experiments. The study of the usefulness and the accuracy of this method at similar experiments was performed with the help of Monte Carlo codes MCNPX and FLUKA.

The investigation has been performed at the Dzhelepov Laboratory of Nuclear Problems, JINR.

Preprint of the Joint Institute for Nuclear Research. Dubna, 2009

## 1. INTRODUCTION

Neutron activation detectors are one of the best options for the measurements of the produced neutron field characteristics in the spallation experiments. Their main advantage is their small size which makes them very useful in the measurements of the spatial distribution of the neutron field. In the Dubna experiments, the neutron activation detectors were mainly used in the form of thin foils and shall be from now on referred to as activation foils to avoid confusion with semiconductor detectors.

The detection of neutrons with activation foils occurs in two steps:

- the neutrons interact with the foil material,
- the activity of radionuclides produced by neutrons in the foil during the irradiation is analyzed.

In the first step, foils are irradiated and part of their material is activated through, e.g.,  $(n, xn)$ ,  $(n, \alpha)$ , and  $(n, \gamma)$  reactions. The new isotopes are unstable, decaying ( $\beta^+$ ,  $\beta^-$ , EC) and emitting characteristic gamma photons. These photons are registered with semiconductor detectors (usually HPGe) in the second step. The amounts of produced isotopes are calculated from the measured activities. The information about the neutron field can also be obtained, providing that the mechanisms of the isotope production are well known.

Gamma spectroscopy is part of many research methods and applications and is covered in several textbooks (for, e.g., [1]). However, there exist some specific problems connected to the use of activation foils in spallation experiments, which are studied in this work. For complete understanding, the derivation of basic spectroscopy equations is shown at the beginning. In the rest of the paper, Monte Carlo simulations are exploited to study the processes around the production and detection of radioisotopes and the accuracy of the neutron activation analysis method in spallation experiments.

## 2. THE PRODUCTION AND DETECTION OF RADIOISOTOPES

Nuclear reactions where neutrons are produced (spallation, direct reactions) usually do not produce monoenergetic neutrons, but time- and space-dependent neutron flux with the energy distribution  $\Phi(E, x, t)$ .

The space distribution of the neutron flux can be measured with small foils placed at different places. The time structure of single-neutron production reactions is usually not measured with this technique, the irradiation should be stable in time (the irradiation is connected with the accelerator output, the correction for unstable accelerator output is discussed in the last sections).

To probe the energetic distribution of neutrons, one has to choose a foil material in which different radioisotopes (each at different neutron energy) are produced.

If an activation material is placed in the neutron flux, a specific radioisotope is produced with the rate  $P$ , and is at the same time decaying with the decay constant  $\lambda = \frac{\ln(2)}{\tau_{1/2}}$ , where  $\tau_{1/2}$  is the half-life of the decay. The rate  $P$  is proportional to the number of available nuclei for the reaction ( $N_0$ ) and the neutron flux  $\Phi(E)$  folded with reaction cross-section  $\sigma(E)$ :

$$P = N_0 \int \Phi(E)\sigma(E)dE. \quad (1)$$

The amount of produced radioisotope is described with the equation:

$$\frac{dN}{dt} = P - \lambda N. \quad (2)$$

The number of produced radioisotopes is zero at the beginning of the irradiation,  $N(0) = 0$ . Assuming the rate  $P$  is constant, the solution to the equation is

$$N(t) = \frac{P}{\lambda}(1 - e^{-\lambda t}). \quad (3)$$

At the end of the irradiation, there are  $N(t_{\text{irr}})$  produced radioisotopes ( $t_{\text{irr}}$  is the irradiation time):

$$N(t_{\text{irr}}) = \frac{P}{\lambda}(1 - e^{-\lambda t_{\text{irr}}}). \quad (4)$$

After the irradiation, the measurements with the HPGe detectors start. The activated material is measured during the time interval  $(t_0, t_0 + t_{\text{real}})$ , where  $t_0$  is the time since the end of the irradiation, and  $t_{\text{real}}$  is the time of the measurement. The number of radioisotopes that decay during this time interval is

$$\begin{aligned} s &= N(t_0) - N(t_0 + t_{\text{real}}) = N(t_{\text{irr}})(e^{-\lambda t_0} - e^{-\lambda(t_0 + t_{\text{real}})}) = \\ &= \frac{P}{\lambda}(1 - e^{-\lambda t_{\text{irr}}})e^{-\lambda t_0}(1 - e^{-\lambda t_{\text{real}}}). \end{aligned} \quad (5)$$

Photons from part of the decayed radioisotopes are detected by the HPGe detector as a gamma peak with the surface  $s$ , which must be corrected to obtain real surface  $S$

$$S = s \cdot \epsilon_P(E) \cdot I_\gamma(E) \cdot \text{COI} \cdot C_g \cdot C_s \cdot C_t \cdot \frac{t_{\text{live}}}{t_{\text{real}}}, \quad (6)$$

where  $\epsilon_P(E)$  is the peak efficiency of the HPGe detector for gamma photons of energy  $E$ ;  $I_\gamma(E)$  is the gamma emission probability (probability that the photon of energy  $E$  is emitted in the decay);  $\frac{t_{\text{live}}}{t_{\text{real}}}$  is the correction for the dead time of the HPGe detector ( $t_{\text{live}}$  is the live time of the measurement); COI is the correction for the decay cascade effect;  $C_g$  is the geometrical correction,  $C_s$  is the correction because of self-absorption of gamma photons in activation foil material, and  $C_t$  is the correction for the beam instabilities during the irradiation. The rate  $P$  is expressed from equations (5) and (6) as

$$P = \frac{S \cdot \lambda}{\epsilon_P(E) \cdot I_\gamma(E) \cdot \text{COI} \cdot C_g \cdot C_s \cdot C_t} \frac{t_{\text{real}}}{t_{\text{live}}} \frac{e^{\lambda t_0}}{(1 - e^{-\lambda t_{\text{irr}}})(1 - e^{-\lambda t_{\text{real}}})}. \quad (7)$$

The number of the produced nuclei of radioisotope  $A$  per one gram of the material and per beam particle is called the production rate  $B(A)$  and is commonly used in the spallation physics studies. The production rate  $B(A)$  can be connected directly with the rate  $P$  (the connection between the neutron flux per time ( $\Phi$ ) and the neutron flux per beam particle ( $\Phi'$ ) is  $\Phi'(E) = \Phi(E) \frac{t_{\text{irr}}}{N_p}$ ):

$$B(A) = \frac{1}{m} \int_E \Phi'(E) \sigma(E) dE = \frac{1}{m} \int_E \Phi(E) \frac{t_{\text{irr}}}{N_p} \sigma(E) dE = \frac{t_{\text{irr}}}{m N_p} P, \quad (8)$$

where  $m$  is the mass of the activation foil, and  $N_p$  is the total number of protons from the accelerator for the spallation reaction. The amount of the produced radioisotope can be expressed also as the reaction rate  $R(A)$ , which is the number of the produced nuclei of radioisotope  $A$  per number of atoms in the sample material and per beam particle. It is connected with  $B(A)$  as

$$R(A) = B(A) \frac{M}{N_A}, \quad (9)$$

where  $M$  is relative atomic mass of the activation foil material, and  $N_A$  is the Avogadro constant.

So far, the irradiation was assumed to be continuous and constant in time. Some accelerators monitor the time structure of their output in regular intervals, and in cases when the output is not constant in time, the time dependency of  $P(t)$  needs to be included in (2):

$$\frac{dN}{dt} = P(t) - \lambda N. \quad (10)$$

The solution is

$$N(t) = e^{-\lambda t} \int_0^t e^{\lambda t'} P(t') dt'. \quad (11)$$

The time structure of the irradiation can be approximated with  $n$  bunches of the beam intensity  $r_i$ , constant in the time intervals  $[t_i, t_{i+1}]$ . With this approximation, the integral in equation (11) is simplified to

$$N(t_n) = \frac{e^{-\lambda t_n}}{\lambda} \sum_{i=1}^n P_i (e^{\lambda t_i} - e^{\lambda t_{i-1}}). \quad (12)$$

The ratio between the number of produced radioisotopes for unstable (11) and stable irradiation (3) is the correction for the beam instability  $C_t$ :

$$C_t = \frac{\frac{e^{-\lambda t_n}}{\lambda} \sum_{i=1}^n P_i (e^{\lambda t_i} - e^{\lambda t_{i-1}})}{\frac{P}{\lambda} (1 - e^{-\lambda t_{\text{irr}}})}. \quad (13)$$

By realizing that  $P$  is proportional to the number of protons in a time interval ( $P = C \frac{N_p}{t_{\text{irr}}}$ ,  $P_i = C \frac{N_i}{t_i - t_{i-1}}$  and  $t_{\text{irr}} = t_n$ ) and by introducing  $W_i = \frac{N_i}{N}$  (number of protons in the bunch  $i$  divided by the total number of protons), factor  $C_t$  can be expressed as

$$C_t = \frac{t_n \sum_{i=1}^n \frac{W_i}{(t_i - t_{i-1})}}{e^{-\lambda(t_n - t_i)} (1 - e^{-\lambda(t_i - t_{i-1})})} 1 - e^{\lambda t_n}. \quad (14)$$

### 3. DETECTION OF RADIOISOTOPES

Emitted gamma photons are detected with HPGe detectors. Photons interact with the detector active material (ca. 120 cm<sup>3</sup>) mainly by photoeffect, Compton scattering and pair production, and can deposit in the detector material their full energy or just a part of it. The response of the detector consists of the peaks at the energies of the emitted photons and the continuum below this energy (Compton edge, escape peaks), see Fig. 8.

The probability that the photon deposits its entire energy in the detector is called full peak efficiency  $\epsilon_P(E)$ , the probability that it deposits any nonzero part of its energy (up to its entire energy) is called total efficiency  $\epsilon_T(E)$ . In equation (7) only peak efficiency  $\epsilon_P(E)$  acts directly, total efficiency  $\epsilon_T(E)$  is however hidden in the COI correction (see Subsec. 3.6), which can range up to ten percents.

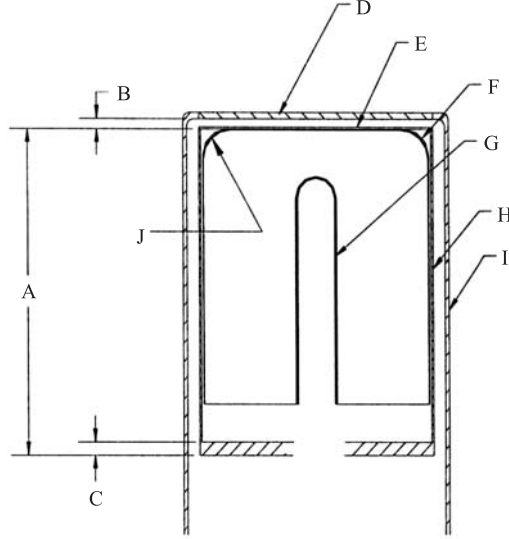


Fig. 1. Extract of the ORTEC GMR-20190-R detector schematic (side cross section). The crystal diameter is 56.8 mm (E), the length 51.3 mm (H), the beryllium window is 0.5 mm thick (D) and the distance from the window to the detector is 3 mm (B). Other dimensions are company secret

The response of HPGe detectors can be reliably predicted with the Monte Carlo codes. The details of the detector inner structure are often company secrets and mainly for this reason the simulated predictions have limited accuracy. In Fig. 1 the detector geometry as was implemented in the MCNPX code package [2] for the simulations of  $\epsilon_P(E)$  and  $\epsilon_T(E)$  efficiencies is shown. The energy deposited in the detector (F8 tally) at incident photons energies in the keV–MeV range was studied. The efficiencies were defined as the ratio between the number of simulated histories at which full/partial energy was deposited in the detector and the number of all histories.

**3.1. Experimental Calibration.** The detectors are experimentally calibrated with radioactive isotope standards. The calibration samples are in the form of small dots of the radioactive isotope, doped on the glass, isotropically radiating photons in all directions. Both the full peak efficiency and the total efficiency are determined at the calibration. The  $\epsilon_T(E)$  can be determined only with the calibration radioisotopes that have one single line in the decay scheme.

The calibration samples with the activity  $A_0$  measured at time  $t = 0$  will undergo  $s$  decays during the calibration time interval  $[t_0, t_0 + t_{\text{real}}]$ :

$$s = N(t_0) - N(t_0 + t_{\text{real}}) = \frac{A_0}{\lambda} e^{-\lambda t_0} (1 - e^{-\lambda t_{\text{real}}}). \quad (15)$$

The measured peak surface  $S$  and the detector efficiency  $\epsilon_P(E)$  are connected with the relation (6), and we can write:

$$\epsilon_P(E) = \frac{S\lambda e^{\lambda t_0}}{A_0 I_\gamma \text{COI} C_g} \frac{t_{\text{real}}}{t_{\text{live}}} \frac{1}{1 - e^{-\lambda t_{\text{real}}}}. \quad (16)$$

The measurement times ( $t_{\text{real}} \approx$  hours) are much smaller than the lifetimes of standard isotopes ( $\tau \approx$  years), therefore,  $e^{-\lambda t_{\text{real}}} \ll 1$ . The last two factors from the previous equation can be simplified by writing  $e^{-\lambda t_{\text{real}}}$  as Taylor series and keeping only the first terms:

$$\frac{t_{\text{real}}}{t_{\text{live}}} \frac{1}{1 - e^{-\lambda t_{\text{real}}}} = \frac{1 - (1 - \lambda t_{\text{real}})}{1 - (1 - \lambda t_{\text{live}})} \frac{1}{1 - (1 - \lambda t_{\text{real}} - \dots)} = \frac{1}{1 - e^{-\lambda t_{\text{live}}}}. \quad (17)$$

Because calibration samples are good approximation of point sources ( $C_g = 1$ ),  $\epsilon_P(E)$  can be written as

$$\epsilon_P(E) = \frac{S\lambda e^{\lambda t_0}}{A_0 I_\gamma \text{COI}} \frac{1}{1 - e^{-\lambda t_{\text{live}}}}. \quad (18)$$

Total efficiency  $\epsilon_T(E)$  is calculated in the same manner, however all counts in the detector up to the peak energy are taken for  $S$  instead of the counts in the peak.

**3.2. Full Peak Efficiency  $\epsilon_P(E)$ .** The peak efficiencies were simulated at approximate distances where the samples are measured during the experiments, see Fig. 2. The simulated peak efficiencies for the 4.1 cm position are shown in Fig. 3, together with the experimentally determined efficiencies (measured with standard calibration radioisotopes). Above 100 keV, the peak efficiencies are reliably fitted with a higher order exponential function of the form:

$$\epsilon_P = e^{a+b \ln(E)+c \ln^2(E)+d \ln^3(E)+\dots} \quad (19)$$

There are a few percent discrepancies between the fitted curve and the measured values. These differences have three different origins: inaccurate placement of the samples (ca. 1 mm inaccuracy), the inaccuracy in the measured activity of the calibration samples (about 2%) and absolute intensity of the gamma line (1%), and the error of the gamma peak fit (1–3%).

The maximum difference between the simulated and fitted experimental curves is below 10% up to the energy of 2000 keV. This means that the detector is well-modelled and that the following simulated results are reliable.

At the measurements of the activation foils with small intensity the close placement of the foil to the detector cannot be avoided. The inaccuracy of the placement has the biggest impact in these positions. The simulations with

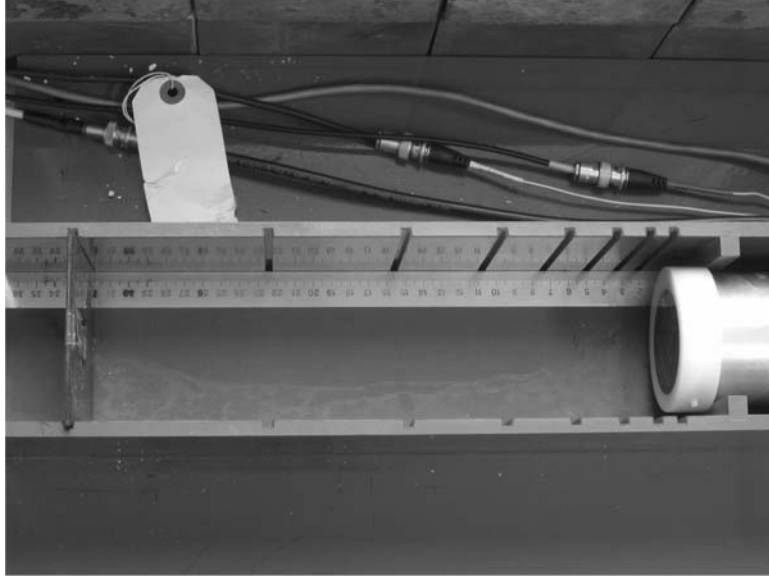


Fig. 2. The holder for foil samples with the detector. The samples are measured at ca. 1.2, 2.4, 4.1, 6.5, 9.9, 14.7, 21.6, 31.1 cm from the detector

the samples placed at 4.0 and 4.2 cm from the detector predict for ca. 3% different results according to the simulation at 4.1 cm. In the position 2.4 cm, the displacement of the source for 1 mm changes the peak area for 4%, and further positions are less sensitive (6.5 cm  $\approx$  2%, further  $<$  1%).

**3.3. Total Efficiency  $\epsilon_T(E)$ .** Figure 4 shows the simulated  $\epsilon_T(E)$ , experimentally determined values and the experimental fit for the position 4.1 cm from the detector. The data are again fitted with a higher order exponential function, usually less factors are needed than for  $\epsilon_P(E)$ .

The isotopes with only one gamma line in the spectrum (or two gamma lines provided that they are close together, e. g.,  $^{57}\text{Co}$ ) can be used for the experimental determination of  $\epsilon_T$ . Only a few calibration samples meet these requirements. The efficiency  $\epsilon_T(E)$  is calculated from equation (18), taking for  $S$  the sum of the signal in all channels up to and including the channels where the peak is registered. In case of longer calibration measurements (for low intensity calibration sources or positions far from the detector) the contribution from the background needs to be subtracted from this value.

The uncertainty of the fitted  $\epsilon_T(E)$  curve is around 15%, because of fewer fitting points and the procedure with the background subtraction. Total efficiency is present in (7) through the cascade coefficient factor (see Subsec. 3.6), which is usually below 5% (10% in rare cases). The  $\epsilon_T(E)$  inaccuracy therefore contributes

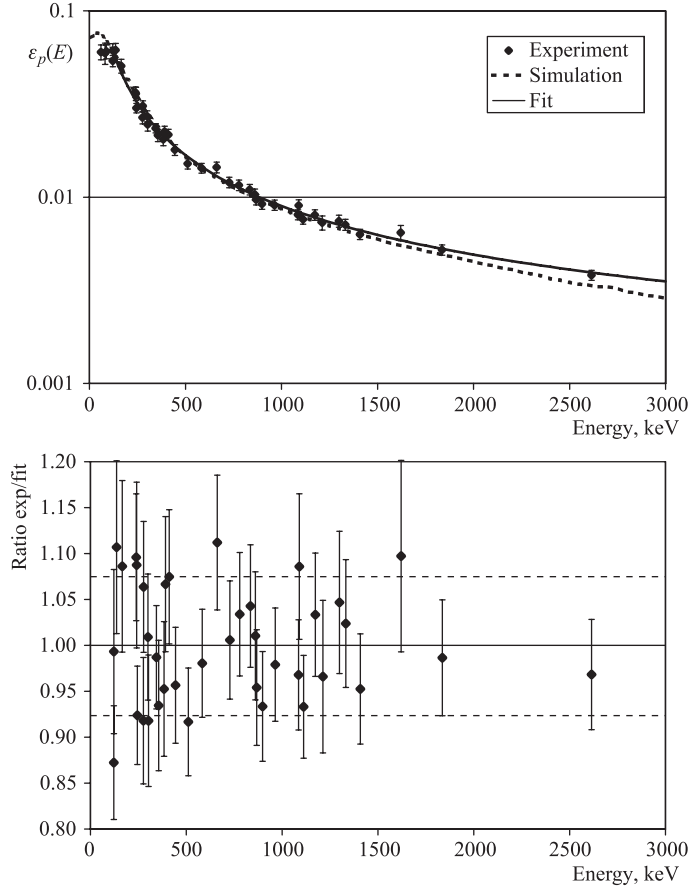


Fig. 3. a) Simulated full peak efficiency ( $\epsilon_P(E)$ ) curve for the ORTEC HPGe detector with experimentally determined efficiencies (the distance from the detector was 4.1 cm) and fitted curve (3<sup>rd</sup> order). b) Ratios between experimental data and the value calculated with the fitted curve. Uncertainties include the inaccuracy of the placement of the measured activity and peak fit

through the cascade coefficient factor  $15\% \cdot 10\% = 1.5\%$  inaccuracy in the overall  $B(A)$  calculation. The difference between the simulated and fitted experimental curves is 30% around 100 keV and decreases to 10% around the energy 3000 keV.

**3.4. Geometrical Correction Factor  $C_g$ .** The calibration samples are point-like dots of radioactive material packed in the sample holder. On the other hand, the activation foils are typically in the form of foils with dimensions  $2 \times 2$  cm and from 50–1000  $\mu\text{m}$  thick (see Subsec.4.3), with the radioactivity distributed

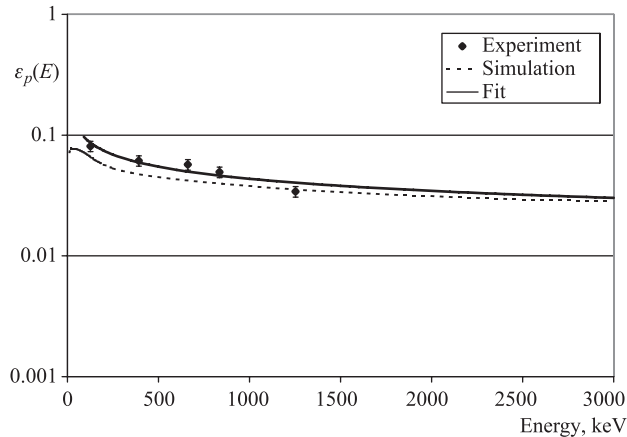


Fig. 4. Simulated total efficiency ( $\epsilon_T(E)$ ) with experimentally determined efficiencies and the fit of experimental values (1<sup>st</sup> order). The distance from the detector was 4.1 cm

in the foil volume. As the photons from the edges of the foil have smaller solid angle covered by the detector, the detector response to the activation foil will be smaller than to the point-like calibration sample with the same activity. The geometrical factor  $C_g$  accounting for this difference is defined as the ratio between the response of the detector to the foil and to the point-like source.

In MCNPX simulations, the geometrical correction factor is then

$$C_g = \frac{\epsilon_P(\text{foil})}{\epsilon_P(\text{point})}, \quad (20)$$

where  $\epsilon_P(\text{foil})$  is the simulated peak efficiency for the activation foil and  $\epsilon_P(\text{point})$  for the point-like source. The simulated peak efficiencies using the sources in form of Al, Au, and Bi foils used in our experiments (Al —  $2 \times 2 \times 0.05$  cm, Au —  $2 \times 2 \times 0.005$  cm, Bi —  $2.5 \times 2.5 \times 0.1$  cm) and subsequently with point-like sources were compared to estimate the geometrical correction factor. Both radioactive sources were placed at the detector positions on 1.2, 2.4, 4.1, 6.5, 9.9, 14.7, 21.6, 31.1 cm (see Fig. 2), the energy of the photons was set to 500 keV. In Fig. 5 it is seen that the geometrical correction factor for larger distances from the detector is approaching to 1. At closer distances it can be as low as 0.92 for the largest Bi activation foils.

The estimation of the geometrical factor from the solid angle under which the source «sees» the detector is also possible. The results of this method are very close to the results of MCNPX simulations, usually within 1%.

The calculation of the geometrical factor with the MCNPX simulation or with the solid angle method can be applied only if at least the crystal radius and the

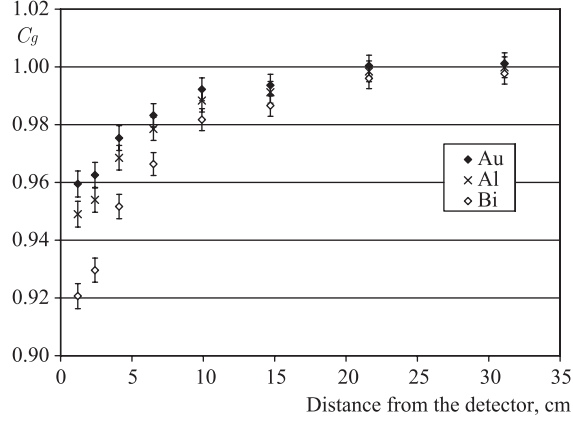


Fig. 5. Geometrical correction factor ( $C_g$ ) in the dependency on the distance from the detector for different foil dimensions (MCNPX simulation)

distance of the crystal from the detector window are known. The inner structure of the detector is often company private, and in such cases another, experimental method has to be used to obtain the geometrical factor. Using the point-like radioactive source, the response of the HPGe detector to the source placed at different radial distances ( $r$ ) from the detector central axis is measured. With the obtained function  $\epsilon_P(r)$ , the geometrical factor is calculated as

$$C_g = \frac{\int_S \epsilon_P(r) dS}{\epsilon_P(0)}. \quad (21)$$

Above-mentioned methods were tested with the experiment performed at the NPI experimental facilities. The  $1 \times 1$  mm (approximating point-like source) and  $2 \times 2$  cm Au foils were irradiated in moderated neutron spectrum and subsequently measured with the HPGe detector at different detector to source distances. The detector responses were compared and obtained geometrical corrections correspond well with the values simulated by MCNPX or calculated with the solid angle method. Using the point-like source, the dependency  $\epsilon_P(r)$  was measured and the value obtained by equation (21) for  $2 \times 2$  cm foil was again in good agreement with the directly measured geometrical correction.

**3.5. Self-Absorption of Gamma Photons in the Activation Foils  $C_s$ .** The mass attenuation coefficients are for activation materials at 100 keV energies in orders of a few  $\text{cm}^2/\text{g}$ . This means that self-absorption in even less than mm thick foils is significant.

The  $C_s$  factor accounts for self-absorption and can be expressed as the ratio between gamma fluxes from the foil with and without self-absorption:

$$C_s = \frac{\int_0^l \frac{I_0}{l} e^{-\mu x} dx}{\int_0^l \frac{I_0}{l} dx} = \frac{1 - e^{-\mu l}}{\mu l}, \quad (22)$$

where  $l$  is the foil thickness and  $\mu$  is the product of attenuation coefficient and foil density. It is assumed that the foil is placed perpendicular to the detector axis and far enough from the HPGe crystal that only photons emitted parallel to the detector axis reach the crystal.

The effect was also studied with the MCNPX simulations. The cases with and without self-absorption were in simulations approximated with foils with volume filled with material and foils filled with air. The source of photons was distributed homogeneously in the foil volume. The efficiency  $\epsilon_P(E)$  of the HPGe detector was simulated for energies of gamma photons ranging from 50–2000 keV and 10–1000  $\mu\text{m}$  thickness of the foil material. The foil with dimensions  $2 \times 2$  cm was placed 2.4 cm away from the detector.

The ratios between the results for foils filled with material and air at different photon energies and foil thicknesses are shown in Fig. 6. The examples of some simulated results for the gold activation foils used at the experiments ( $2 \text{ cm} \times 2 \text{ cm} \times 0.05 \text{ mm}$ ) are shown in Table 1.

The results of  $C_s$  calculation from equation (22) and the MCNPX simulation were identical within statistical errors for all isotopes usually observed in activation foils at spallation experiments.

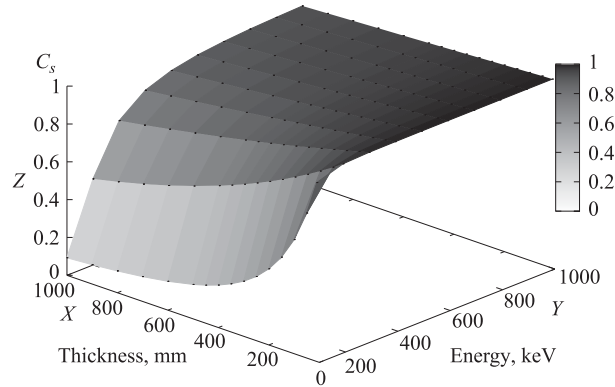


Fig. 6. MCNPX simulation of the self-absorption coefficient  $C_s$  for gold activation foil. On the  $X$  axis is the thickness of the foil, on the  $Y$  axis is the energy of the gamma photons, and on the  $Z$  axis is the self-absorption coefficient

**Table 1. Simulated factors  $C_s$  in gold foils. The foil dimensions used in simulation were  $2\text{ cm} \times 2\text{ cm} \times 0.05\text{ mm}$**

| Radioisotope      | Energy, keV | $C_s$   |
|-------------------|-------------|---------|
| $^{195}\text{Au}$ | 98.85       | 0.762   |
| $^{193}\text{Au}$ | 186.17      | 0.945   |
| $^{194}\text{Au}$ | 293.545     | 0.981   |
| $^{196}\text{Au}$ | 332.983     | 0.985   |
| $^{198}\text{Au}$ | 411.80205   | 0.990   |
|                   | above 420   | > 0.990 |

**3.6. Cascade Coincidences.** The  $\gamma$  decay of an excited nucleus goes through several excited levels, emitting photons or conversion electrons at each step. At a single decay, several photons can be emitted at different angles and they can also deposit their energy in the detector simultaneously. This effect is known as cascade coincidence.

True coincidences occur when two or more cascading photons — emitted in the decay of a radionuclide with negligible time delay — give rise to a total or partial energy deposition in the detector.

Two or more photons registered in the detector can also be from different decays — false coincidences. Such coincidences are usually negligible. Only in the case when the intervals between the hits are smaller than the detector dead time (few  $\mu\text{s}$ , activities in orders of MBq), they should be taken into account.

The probability that more photons are emitted to solid angle towards the detector decreases with the distance from the detector, and true coincidences are significant only at small source to detector distances.

Cascade coincidences can change the area under gamma peaks in two ways:

- Several photons from the decay deposit their energy in the detector together. The area of the observed peaks is smaller for a factor  $L$  (see (24)), the energy is deposited in channels corresponding to higher energies. Smaller peaks and corresponding background arise at the sum of the energies of photons, see Fig. 8.

- The nucleus can decay from one state to another directly by emitting one photon or in several steps, emitting photons at each step. The sum of the photon energies corresponds to the energy of the photon in the single step. If all photons fully deposit their energy in the detector, the peak area of the single-step photon will be increased for a factor  $S$  (see (25)).

Corrections for cascade coincidences can be avoided if the same radioactive isotopes are used for the calibration and for the measurement. The correction can also be determined experimentally with the measurements at different distances from the detector. The cascade coincidences at large distances are negligible (the probability that two photons from the same decay are emitted into the solid angle towards the detector is small).

The basic calculation procedure of the correction factor is described elsewhere [2, 3]. In brief, the correction factor, for example, shown in Fig.7, is given as

$$\text{COI} = (1 - L)(1 + S), \quad (23)$$

where coefficients  $L$  and  $S$  are

$$L(B) = a_C c_C \epsilon_T(C), \quad (24)$$

$$S(A = B + C) = \frac{I_B}{I_A} a_C c_C \frac{\epsilon_P(B) \epsilon_P(C)}{\epsilon_P(A)}. \quad (25)$$

Factor  $c_C = (\alpha_C + 1)^{-1}$  is the probability that the photon will be emitted at the transition (conversion electron is another possibility,  $\alpha_C$  is the conversion coefficient and is the ratio between the irradiation probabilities of the conversion electron and gamma photon), and  $a_C$  the probability that the transition  $C$  will happen from all possible transitions from a given state ( $a_C = 1$  in our case, but for, e.g.,  $a_B = \frac{I_B/c_B}{I_A/c_A + I_B/c_B}$ ). These equations can be extended for decays through more excited states, see for, e. g., [3].

Another method was proposed by T.M.Semkow et al. in [4]. The authors introduced a vector of feeding factors  $\mathbf{f}$ :

$$\mathbf{f} = (f_0 f_1 \dots f_n), \quad (26)$$

where  $f_i$  is the  $i$ th level feeding factor. The total branching ratios are designated as  $x_{ji}$  for a transition from level  $j$  to  $i$ , and form a square lower-triangular matrix  $\mathbf{x}$ :

$$\mathbf{x} = \begin{pmatrix} 0 & & & & & \\ x_{10} & 0 & & & & \\ x_{20} & x_{21} & 0 & & & \\ \vdots & \vdots & \vdots & & & \\ x_{n0} & x_{n1} & x_{n2} & \dots & x_{nn-1} & 0 \end{pmatrix}. \quad (27)$$

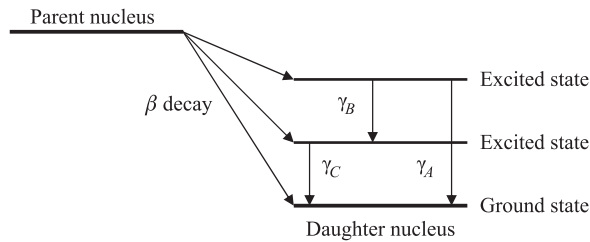


Fig. 7. Decay scheme with lines A, B, and C

Other matrices  $\mathbf{c}$ ,  $\mathbf{a}$ ,  $\mathbf{e}$ , and  $\mathbf{b}$  are defined below and their elements are functions of  $x_{ji}$  as well as of the peak efficiencies  $\epsilon_P(E_{ji})$ , the total efficiencies  $\epsilon_T(E_{ji})$ , and the total  $\gamma$ -ray conversion coefficients  $\alpha_{ji}$ :

$$c_{ji} = \frac{x_{ji}}{1 + \alpha_{ji}}, \quad a_{ji} = c_{ji}\epsilon_P(E_{ji}), \quad e_{ji} = c_{ji}\epsilon_T(E_{ji}), \quad b_{ji} = x_{ji} - e_{ji}. \quad (28)$$

Matrices  $\mathbf{A}$  and  $\mathbf{B}$  are introduced:

$$\mathbf{A} = \sum_{k=1}^n \mathbf{a}^k, \quad \mathbf{B} = \mathbf{E} + \sum_{k=1}^n \mathbf{b}^k, \quad (29)$$

where  $\mathbf{E} = \text{diag}(1)$  is a unit matrix. A consecutive  $k$ -times multiplication of a matrix is abbreviated as the matrix to the  $k$ th power. Two diagonal matrices  $\mathbf{N}$  and  $\mathbf{M}$  are functions of  $\mathbf{B}$ :

$$\mathbf{N} = \text{diag}([\mathbf{fB}]_i), \quad \mathbf{M} = \text{diag}(B_{i0}). \quad (30)$$

The cascade coincidence factors  $S_{ji}$  form a matrix  $\mathbf{S}$ :

$$\mathbf{S} = \mathbf{N} \cdot \mathbf{A} \cdot \mathbf{M}. \quad (31)$$

This notation should be equivalent to formulas obtained by the basic calculation procedure.

**3.6.1. The Simulations of Cascade Coincidences with the FLUKA Monte Carlo Code.** For the simulations of the cascade coincidences, a source which emits more photons in a single history needs to be implemented in the code. The implementation to MCNPX turned out very difficult, while the FLUKA code [?, ?] already contains subroutines, which were only slightly changed to emit more photons in one history. The electromagnetic part of the FLUKA code is almost identical to the one in the MCNPX code, what was also verified with some simulations from the previous sections that were repeated with FLUKA and the same results within statistical uncertainties were obtained.

For cascade coincidence related simulations, the detector was simplified with a Ge cylinder with 4 cm diameter and 5 cm length. Both efficiencies ( $\epsilon_T$  and  $\epsilon_P$ ) were simulated for a few distances of the radioactive source from the detector (1, 5, 10 cm), and calculated efficiencies were fitted with appropriate exponential functions (Subsecs. 3.2 and 3.3).

In the next step, FLUKA subroutine *source.f* was modified to release in each history one of the photons from the studied radioactive decays (radioactive isotopes  $^{60}\text{Co}$  and  $^{133}\text{Ba}$  were studied). The probabilities of the choice of the emitted photon energy were set to absolute intensities of the gamma lines, taken from the ENDL database [5]. The spectrum of the energy deposited in the detector corresponds to the theoretical case where there are no cascade effects (Fig. 8).

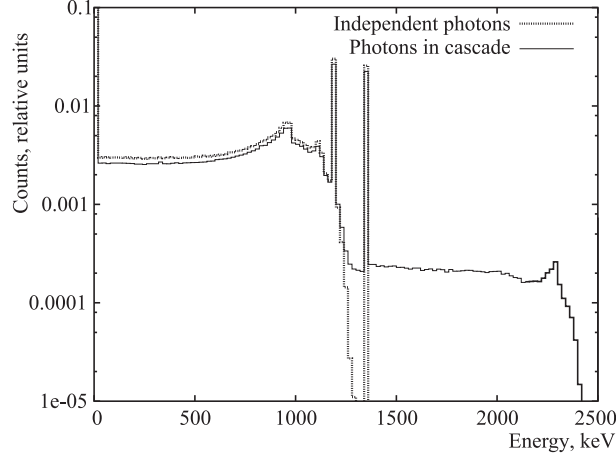


Fig. 8. FLUKA simulation of the detector response to the  $^{60}\text{Co}$  source placed 1 cm from the detector front. For the case when two photons are in cascade, the area under the peaks is decreased (for the factor COI) and another peak at the sum of the energies of both photons appears

The subroutine *source.f* was then modified to emit more photons in the same history (as in the real radioactive decay) and the response of the detector was simulated. Two cases were simulated, the first one with both photons emitted isotropically (without the correlation between their directions) and the second with the correlation between the angular distribution of emitted photons. The distribution of solid angles between the photons is generally defined by the equation

$$W(\theta) = \sum_{\nu} A_{\nu}^{(1)} A_{\nu}^{(2)} P_{\nu}(\cos \theta), \quad (32)$$

where  $P_{\nu}$  are Legendre polynomials, and coefficients  $A_{\nu}^{(1)}$  and  $A_{\nu}^{(2)}$  are functions of multiplicities and spins of the radiations. The detailed explanation of the angular distribution correlation is beyond the scope of this work, and can be found in textbooks, e.g., [6]. For example, in the decay of isotope  $^{60}\text{Co}$  two photons are emitted and the distribution of the solid angle between them is correlated with the following function:

$$\begin{aligned} W(\theta) &= 1 + A_2 P_2(\cos \theta) + A_4 P_4(\cos \theta) = \\ &= 1 + 0.1020 \frac{1}{2} (3 \cos^2(\theta) - 1) + \\ &+ \frac{0.0051}{8} (35 \cos^4(\theta) - 30 \cos^2(\theta) + 3). \end{aligned} \quad (33)$$

The spectra from different simulation steps were compared to the spectrum with one photon in each decay, and the correction for the cascade effects

was defined as

$$\text{COI} = \frac{S_r}{S_1}, \quad (34)$$

where  $S_1$  is the area under the peak obtained with the simulation where one photon was emitted in the history, and  $S_r$  is the same area for the simulated realistic decay.

At the closest distance of the radioactive source from the detector (1 cm), the correction for cascade effects was up to 12%. The factors simulated with angular correlation differ for less than 1% from the factors without angular correlation. The simulation with angular correlation was repeated with the first multiplier ( $A_2$ ) set to 0.3 instead of 0.1020. For the big majority of decays 0.3 is the upper limit for this multiplier [7]. The factors calculated with  $A_2 = 0.3$  differ for 2% from the correction factor without angular correlation.

The COI corrections at the distance 5 cm are less than 5% and at the distance 10 cm less than 2%. The numbers calculated with FLUKA code were compared to the numbers obtained by two analytical calculation procedures mentioned in the previous sections. Simulated  $\epsilon_T$  and  $\epsilon_P$  were used in equations (23)–(31). For both studied isotopes ( $^{60}\text{Co}$  and  $^{133}\text{Ba}$ ) the identical results (comparing to FLUKA simulation without angular correlation) for COI corrections were obtained within 0.5%. It should be noted that analytical procedures do not include angular correlations between emitted photons, but the corrections because of these correlations are small ( $\approx 1\%$ ).

## 4. PRODUCTION OF RADIOISOTOPES

**4.1. Spectra of Produced Particles and Cross Sections.** Beside neutrons, the following particles are produced in the spallation reaction: protons, photons, pions and heavier fragments ( $d, t, \dots$ ). These particles all contribute to the production of the measured radioisotopes, and it is important to have a figure on their influence.

The example of the calculated spectra of the particles produced in the spallation is seen in Fig. 9. The spectra of neutrons, protons, deuterons, charged pions, and photons were calculated with MCNPX, with 1 GeV deuteron beam directed to the lead target of 50 cm length and 5 cm radius. Another simulation with the same target surrounded by 2 m of water (moderator) is referred to as «water bath» case. At experiments, targets are placed in the moderating environment (concrete walls, soil), and neutron spectrum obtained in the «water bath» simulation should be closer to the reality than in the bare target case. The influence of the moderator on the spectra of other particles is negligible. From Fig. 9 it is seen that mostly neutrons are produced, the production of protons and photons is suppressed for one order of magnitude (protons — Coulomb barrier, photon emission

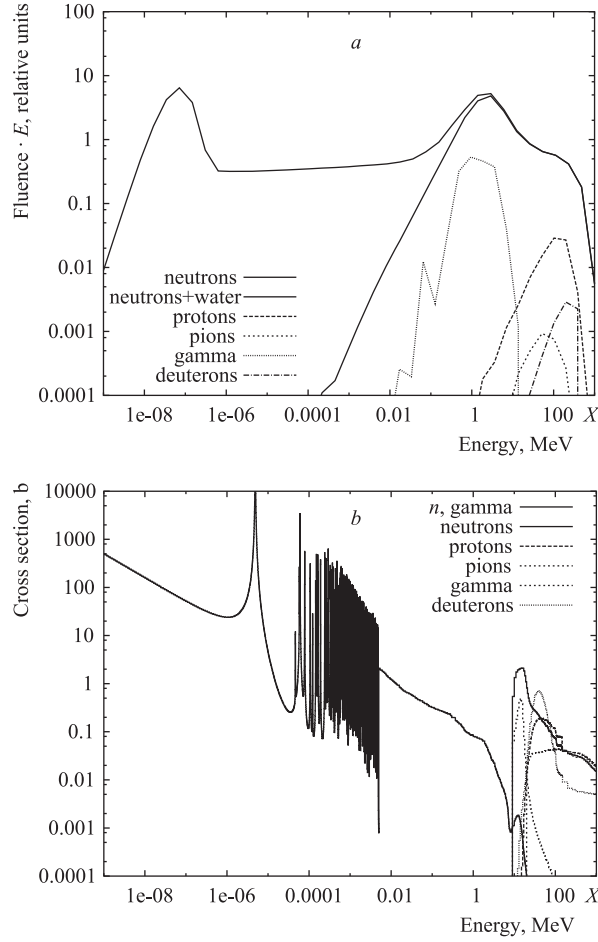


Fig. 9. Spectra of produced secondary particles in the spallation reaction (a). The beam of 1 GeV deuterons was directed to the lead target (50 cm length, 5 cm radius). The neutron spectrum simulated with the target surrounded by 2 m of water is referred to as «neutrons + water». Cross sections for reactions with neutrons, protons, photons, pions, and deuterons in which  $^{196}\text{Au}$  is produced (b). The energy scale ( $X$  axis) corresponds to the spectra presented above. Cross sections were calculated with TALYS 1.0 code, with the exception of pions (MCNPX code, CEM03 model) and data for  $(n, \gamma)$  reaction [8]

competes with neutron emission only in the last phase of the spallation reaction), the production of pions is strongly suppressed in our beam energy range.

The produced neutrons interact with the activation material through  $(n, xn)$  and  $(n, \gamma)$  reaction channels, protons through  $(p, p(x-1)n) \dots$  An example of the

cross sections for  $^{197}\text{Au}(n, 2n)^{196}\text{Au}$  reactions (and their equivalents that produce the same radioisotope with protons, pions, and photons) are shown in Fig. 9. Reactions  $(n, xn)$  with higher  $x$  have similar shape of the cross sections, but the threshold is placed towards higher energies (thresholds for  $(n, 2n)$ ,  $(n, 3n)$ ,  $(n, 4n)$  reactions are 8.1, 14.8, 23.2 MeV). Another reaction with similar shape of the cross sections is  $(n, \alpha)$  in Al with the threshold at 3.2 MeV. Low energy neutrons ( $0.1 \text{ eV} < E_n < 0.1 \text{ MeV}$ ) which are not produced in the spallation reactions in large quantities (but there is always plenty of them as a result of the moderation in the shielding materials or moderator) interact with the activation material with  $(n, \gamma)$  reactions.

**4.2. Influence of Other Particles.** The production rates  $B(A)$  are obtained by folding the spectra and appropriate cross sections from Fig. 9. The particles other than neutrons will give small but not negligible contribution to the total production rate. At the typical (for spallation experiments) beam energy of 1 GeV, the contribution from photons and pions can be usually neglected, as they contribute less than 1%. On the other hand, proton and deuteron (in the case where a deuteron beam is used) contributions are not negligible. Primary protons (deuterons) from the beam are mostly responsible for proton (deuteron) induced reactions, and their contribution vary significantly with the placement of the activation foils. In the positions reached by primary particles, these contributions can be up to tens of percents as shown by simulation.

In the simulation, the target was divided into two parts (15 + 35 cm) with 1 mm gap between them. The 1 GeV narrow, deuteron beam was directed to the target and spectra sampled in the gap were folded with the appropriate cross sections. It was found out that, e.g., 20% of radioisotope  $^{192}\text{Au}$  was produced with protons, 5% with deuterons, while pion and photon contributions were below 1%.

Therefore, the contributions to  $B(A)$  from the reactions with other particles should always be considered at the spallation experiments. The same is valid for reactions of type  $(n, f)$ ,  $(n, \alpha)$  . . . in other activation materials. The exception is  $(n, \gamma)$  reaction, which is sensitive to low energy neutrons only ( $0.1 \text{ eV} < E_n < 0.1 \text{ MeV}$ ).

**4.3. Dimensions of the Foils.** The minimal mass of the foil material is determined by the number of activated nuclei that can be detected with the HPGe detector. The gamma peak from the radioisotope should be visible in the spectrum background, which usually increases with the rate about at least 1 count/minute in a channel around the energy 500 keV.

In our commonly used conditions, after one hour of the background measurement, the expected number of counts in that channel will be with 98% probability  $60 \pm 3\sigma = 60 \pm 3\sqrt{60} = 60 \pm 23$ . The count rate from the radioactive isotope in one channel should be more than 23 counts per hour if it should be distinguishable from the background. Because the energy resolution of the detector is around 2–3 keV, the peak can be registered in the neighbor channels covering

2–3 keV range, what is around 10 channels in our case. In these channels more than 23 counts per hour are required, in total  $\approx 230$  counts (for this estimation the peak is approximated with a step function and not with the Gaussian function).

The background usually grows much faster when the radioactive material is measured. Setting at least 1000 counts per hour in the peak for the lowest detectable limit is a realistic estimation in our case.

The peak efficiency of the HPGe detector around the energy 500 keV is around 1% (Subsec. 3.2). If a photon is emitted at every decay of the radioactive isotope and 1000 counts should be registered during one hour, approximately  $2 \cdot 1000 \cdot \frac{1}{1\%} = 200000$  nuclei need to be activated, assuming that  $\tau_{1/2} = 1$  hour\*. In practice, there are more foils to be measured with the HPGe detector, and most of them are not measured immediately after the irradiation, but a few decay periods after it. Usually, one order-of-magnitude higher number of activated radioisotopes during the irradiation is necessary for the reliable measurement.

For example, at the spallation experiments performed at JINR,  $B(A)$  rates are in orders of  $10^{-6} \text{p}^{-1}$  and proton integrals are  $10^{13}$ . This means that in 1 g of the material  $10^7$  radioisotopes will be produced during the irradiation, what is easily measured. The activation material is in the form of thin foils with sides  $2 \times 2$  cm and thickness from 50  $\mu\text{m}$  up to 1 mm. The masses of such foils are 0.4–6 g.

**4.3.1 Small Foils.** The foil is supposed to be small, so that the measured quantity does not change considerably in different parts of the foil. The simulations of the experiments discussed in [9, 10] showed that the changes in the neutron flux on the cm scale can be as high as 50%. This is much more than the accuracy of the activation method and foils with the dimensions on the cm scale cannot be considered as small. The foils on the mm scale are small at such experiments.

In the simulations the foil dimensions can be implemented and the neutron flux can be averaged over the whole place of the foil. That compensates for the fact that the foils are not small when simulated values are compared with experimental results. As more foils are usually placed next to each other in experiments, the measured values can also be interpolated.

**4.3.2 Thin Foils.** The foils should be thin enough not to disrupt the measured neutron fluxes. In general, even 1 mm thick activation foils are thin enough for MeV neutrons (cross sections for  $(n, xn)$  reactions are maximally in orders of barns), but not for low energy neutrons (cross sections for  $(n, \gamma)$  reactions are up to thousands of barns).

---

\*Counts = decays  $\cdot \epsilon_P$ , decays =  $N_0 - N_0 e^{-\lambda \tau_{1/2}} = \frac{1}{2} N_0$ .

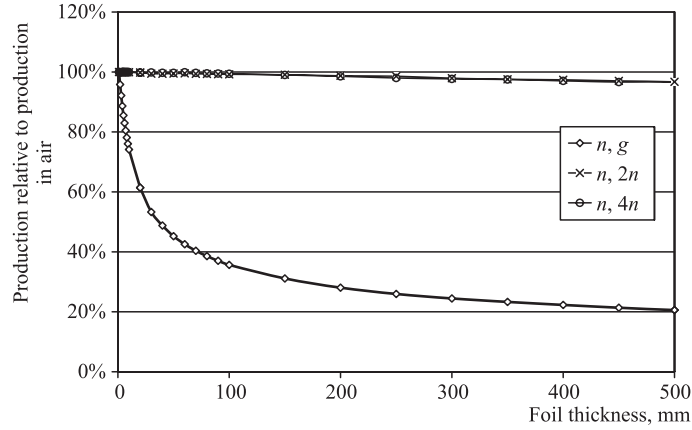


Fig. 10. Ratio between the production rates for  $(n, xn)$  and  $(n, \gamma)$  reactions in the gold foils with different thicknesses and the production rates in the foils filled with air (no absorption). The neutron spectrum from Fig. 9 (water bath case) was used in the simulation

The simulation with the neutron spectrum from Fig. 9 (water bath case) directed to the gold activation foils with thicknesses from  $10 \mu\text{m}$  up to 1 mm was performed. The neutron spectra sampled in the gold foil were folded with cross sections for  $(n, xn)$  and  $(n, \gamma)$  reactions. While in the case of  $(n, xn)$  reactions the obtained production rate did not change, in the case of  $(n, \gamma)$  reaction the production rate decreased significantly with the thickness, see Fig. 10. The experiment with Au foils wrapped one in another and irradiated at the NPI cyclotron (Řež) confirmed the result of the simulation. Again, the absorption is taken into account in the simulations if the foil dimensions are properly implemented. For experimental data, the factor for which the production rates are lower due to absorption can be calculated. This conclusion can be applied also to other reactions which have similar cross sections to  $(n, \gamma)$ , for example  $(n, f)$  reactions.

**4.3.3 Transport of Activated Material out of Foil.** In the case of very thin foils, the loss of activated material from the foil can also become significant and needs to be discussed. At the  $(n, xn)$  reaction, the activated nucleus can obtain the kinetic energy up to few tens of MeV. Such nuclei can have the range of few  $\mu\text{m}$  in the foil material (calculated with SRIM code [11]), and can move out of the foil during the irradiation.

The irradiation of the  $50 \mu\text{m}$  gold foil with quasi-monoenergetic neutron beam of 36 MeV at the NPI cyclotron was performed to study such transport. The foil was wrapped in thick paper and scotch tape envelope, which should stop all the escaped radioisotopes. The paper and the foil were measured separately and the number of the nuclei in the paper was 4 orders of magnitude lower than in

the foil. The escape of the radioisotopes can therefore be considered as negligible. In any case, it can be avoided by packaging the foils in envelopes that stop the escaping fragments.

## CONCLUSION

The neutron activation detectors are widely used at the spallation experiments. They cover a wide energy scale from tens of MeV down to thermal energies. For their small size they can be applied almost everywhere, and the analysis of the experimental data is relatively easy. Their disadvantages are the limited accuracy of the obtained results and several corrections that need to be taken into account.

In this work, a review of the activation detector method is given and some known facts are being reconsidered in the special case of spallation experiment: corrections have to be applied if the activation detectors cannot be approximated as small and thin detectors (attenuation of neutrons in the detector material), most radioisotopes that are found by the gamma analysis are not produced only by neutrons but also by other particles resulting from the spallation, etc. With the help of Monte Carlo simulations it is shown that the main source of the systematical error during the irradiation is the misplacement of the foils. At most experiments, the measured quantities depend strongly on the position, and the detectors should be placed with the millimeter accuracy to obtain accurate results.

After the irradiation of the activation detectors with neutrons, they are analyzed with the gamma-spectrometry method, which is another source of inaccuracies. The calibration of the HPGe detectors is accurate up to a few % (in the best case 5%). At closer detector to foil distances, one should count with the misplacement of the foil, which causes another 2–3% inaccuracy as was shown with simulations. Other numerous corrections are discussed and are well-understood and controlled, the uncertainties caused by them should not exceed 1–2%. With the uncertainties connected with the fitting of gamma peaks, the total accuracy of the gamma-spectrometry method is slightly below 10%.

**Acknowledgements.** The access to the METACentrum computing facilities provided under the research intent MSM6383917201 is appreciated. This work was carried out partly under support of the Grant Agency of the Czech Republic (grant No. 202/03/H043) and IRP AV0Z10480505 (the Czech Republic).

## REFERENCES

1. *Gilmore G.* Practical Gamma-Ray Spectroscopy. CHIPS, 2008.
2. *Andrew D. S. et al.* // Instr. Exp. Tech. 1972. V. 15. P. 1358.

3. *De Corte F.* The k0-Standardization Method. A Move to the Optimization of Neutron Activation Analysis. Rijksuniversiteit Gent: Faculteit van de wetenschappen. 1986. P. 75.
4. *Semkow T. M. et al.* // Nucl. Instr. Meth. Phys. Res. A. 1990. V. 290. P. 437–444.
5. *Chu S. Y. F. et al.* WWW Table of Radioactive Isotopes. 1999. V. 2/28.  
<http://nucleardata.nuclear.lu.se/nucleardata/toi>.
6. *Siegbahn K.* Alpha-, Beta- and Gamma-Ray Spectroscopy. Amsterdam: North-Holland Publishing Company, 1965.
7. *Drahoslav V.* Multi-Detector Spectrometer MUK with Ge(Li)-Detectors for Space-Time Correlation of Nuclear Radiation. PhD Thesis. JINR. Dubna, 1991 (in Russian).
8. *Chadwick M. B. et al.* ENDF/B-VII.0: Next Generation Evaluated Nuclear Data Library for Nuclear Science and Technology // Nucl. Data Sheets. 2006. V. 107. P. 2931–3060.
9. *Majerle M. et al.* JINR Preprint E15-2008-94. Dubna, 2008.
10. *Majerle M. et al.* JINR Preprint E15-2007-72. Dubna, 2007.
11. *Ziegler J. F. et al.* The Stopping and Range of Ions in Solids. N. Y.: Pergamon, 1985.

Received on October 19, 2009.

Корректор *Т. Е. Попеко*

Подписано в печать 18.03.2010.

Формат 60 × 90/16. Бумага офсетная. Печать офсетная.

Усл. печ. л. 1,68. Уч.-изд. л. 2,29. Тираж 320 экз. Заказ № 56939.

Издательский отдел Объединенного института ядерных исследований  
141980, г. Дубна, Московская обл., ул. Жолио-Кюри, 6.

E-mail: [publish@jinr.ru](mailto:publish@jinr.ru)

[www.jinr.ru/publish/](http://www.jinr.ru/publish/)